J Mater Sci: Mater Electron (2016) 27:4711–4722
DOI 10.1007/s10854-016-4351-6

Influence of ammonia sources on the gas sensing properties of the direct grown ZnO nanomaterials

Xianqing Tian[1] · Kun Yu[1] · Xinfeng Wang[1] · Li Yang[2] · Jie Sun[1]

Received: 11 October 2015 / Accepted: 15 January 2016 / Published online: 29 January 2016

Abstract ZnO nanomaterials have been directly grown on Al_2O_3 ceramic tube by two step seeds-assisted solution method with different ammonia sources. The crystalline phase and morphology of the ZnO nanomaterials are characterized by XRD and SEM. The results of SEM reveal that the ZnO nanomaterials present different morphologies and hierarchical structures where rhombus-shaped nanoprisms, nanorods assembled nanoflowers and nanoleaves constructed nanourchins are obtained in NH_4F, hexamethylenetetramine (HMT) and urea, respectively. All of the ZnO nanomaterials show the optimal working temperature at 320 °C and excellent repeatability. Gas sensing experiments demonstrate that the ZnO nanomateirals perform high responses and fast response-recovery to volatile organic compounds, especially for the nanorods assembled nanoflowers prepared in the HMT. It is believed that the enhancement of the gas sensing performances is mainly attributed to the hierarchical structures, exposed deficiencies and excellent ohm contact of the direct grown ZnO nanomaterials.

✉ Xinfeng Wang
wxplain@sina.com

✉ Jie Sun
zhuoshisun@163.com

[1] Institute of Chemical Materials, China Academy of Engineering Physics, Mianyang 621900, People's Republic of China

[2] SiChuan HaiTian Industry Co. Ltd, Mianyang 621900, People's Republic of China

1 Introduction

As a typical metal oxide semiconductor, zinc oxide (ZnO), with a wide band gap (3.3 eV) [1], shows good morphology tailoring properties, high electron mobility, good chemical stability and low production cost, which are all desirable characteristics for gas sensor. Previous reports have demonstrated that ZnO exhibits good response characteristics to many toxic gases like NO_2 [2–5], CO [6–8], NH_3 [9, 10], H_2S [11–14] and volatile organic compounds (VOCs) [15–18]. It is also confirmed that ZnO nanomaterials with 2D or 3D nanostructures may have a potential to develop high performance gas sensors owing to their large surface-to-volume ratio, especially for the hierarchical nanostructures [19–25]. Many researches have been evoked to synthesis ZnO nanomaterials with different structures, such as nanosheets [19, 26–29], nanolamellaes [30], nanoflowers [19, 21], microwires [31, 32], tetrapods [33]. However, the outstanding gas sensing performances of ZnO nanostructures could not be fully shown through the conventional sensor processing, and thus the gas sensitivity of such ZnO crystal-based gas sensor is deeply restricted by the fabrication process [34], in which these obtained ZnO nanomaterials have difficulties in preserving their nanostructures. Recently, gas sensors based on direct growth of ZnO nanomaterials on the sensor surface have begun to attract the interest of researches due to the easy operating and high sensing performances [26, 27, 34, 35]. For example, Ju et al. [27] have directly grown ZnO nanosheets on Al_2O_3 sensor surface by one-step hydrothermal method. And the obtained ZnO nanosheets presented an excellent response to ethanol at 400 °C. Tian et al. [34] fabricated ZnO nanorods array by a dip-coating method which proved to be an effective way to investigate the exposed-facet-related gas sensing mechanism.

Comparison demonstrated a gas sensor based on direct grown ZnO nanomaterials was more excellent than that based on conventional coating process [27, 28]. However, compared to sensors constructed via conventional coating process, sensors fabricated by directly growth of ZnO nanomaterials and research on their gas sensing properties are still at an early stage. Thus, an in-depth research on the sensors by direct growth of ZnO nanomaterials and exploration of their sensing properties are necessary.

Ammonium fluoride (NH_4F) [36], hexamethylenetetramine (HMT) [37], urea [24], ethylenediamine [26] and so on, are common ammonia sources that have been widely utilized in the wet methods of ZnO preparation, which have also been proved to be an important factor that influences the ZnO sensors' gas sensing performances. However, most of the literatures based on the direct grown ZnO nanomaterials on sensor surface are focusing on HMT or ethylenediamine. It is necessary to investigate the effect of different ammonia sources that impacts the ZnO sensors' gas sensing properties. In this work, the direct growth of ZnO nanomaterials on Al_2O_3 tubes has been formulated in NH_4F, HMT and urea growth systems. The as-prepared ZnO nanomaterials present different morphologies and hierarchical structures where rhombus-shaped nanoprisms, nanorods assembled nanoflowers and nanoleaves constructed nanourchins are obtained in NH_4F, HMT and urea growth system, respectively. The gas sensing experiments reveals that the ZnO nanomateirals have excellent responses to VOCs especially that prepared in the HMT shows the highest response. It is believed that the hierarchical structures and more exposed deficiencies result in the significant enhancement of the gas sensing performances.

2 Experimental

2.1 Chemicals and materials

Analytical grade zinc acetate dihydrate ($Zn(CH_3COO)_2 \cdot 2H_2O$), Zinc nitrate hexahydrate ($Zn(NO_3)_2 \cdot 6H_2O$), ammonium fluoride (NH_4F), hexamethylenetetramine (HMT), urea, methanol, ethanol, acetone and acetonitrile were purchased from Chengdu Kelong Co. (China) and used as received without any further purification. Ultrapure water was used throughout the experiment. The Al_2O_3 ceramic tubes imprinted with two gold electrodes were obtained from Winsen Technology Co. (China) and ultrasonically cleaned before use.

2.2 Direct growth of ZnO nanomaterials on sensor surface

The direct growth of ZnO nanomaterials on ceramic tubes was carried out through seeds-assisted protocol with some modification [26, 27, 34–36]. Generally the protocol contains two steps, the seeds preparation on the surface of the Al_2O_3 ceramic tubes and the growth of ZnO nanomaterials. In the seeds preparation step, 0.02 M $Zn(CH_3COO)_2$ solution was used as the seeds solution. The cleaned Al_2O_3 ceramic tubes were immersed into the seed solution for 10 min followed with calcination at 500 °C for 3 h. After cooled down to room temperature, the seeds implanted ceramic tube was prepared. In the ZnO grown step, the chemicals used to make growth solution include $Zn(NO_3)_2$ (0.025 M), HMT (0.025 M) (or 0.10 NH_4F, or 0.05 M urea) and ultrapure water. Then the seeds implanted ceramic tubes were hung in the growth solution using a stainless steel wire. After that, the growth solution was heated to 90 °C to fulfill the growth of ZnO nanomaterials. After certain duration, the tubes were pulled out and washed with ultrapure water and ethanol, respectively. After being dried under ambient atmosphere, the tubes were annealed in a muffle furnace at 300 °C for 3 h in air. Finally the tubes were naturally cooled to room temperature and stored in atmosphere for further use.

2.3 Characterization of the ZnO nanomaterials

The crystallographic structure of the sample on the ceramic tube was analyzed by a Bruker D8 Avance X-ray powder diffractometer (XRD) with Cu-Kα radiation operating at 30.0 kV and 20.0 mA. A scanning electron microscopic (SEM) image was obtained from a CamScan Apollo 300 SEM.

2.4 Fabrication and measurement of the ZnO sensors

A Ni–Cr heating wire was inserted into the ceramic tube and welded together with the Pt wires to the substrate to form a side-heated gas sensor. The sensing performances were measured using a Winsen WS-60A gas sensor test system interfaced to a personal computer. Before the gas sensing measurements were performed, all of the as-prepared gas sensors were plugged into the sockets of a Winsen TS-60 aging system to be aged electrically (320 °C) in air for 10 days. After a stable response was obtained, the as-prepared sensors were placed in a chamber and connected to the WS-60A for the gas sensing measurements. A detailed schematic diagram of the gas sensing setup could be found in our previously report [38].

In this study, the static volumetric method was utilized to generate different concentrations of VOC vapors to evaluate the sensing performances of the ZnO gas sensors. The static volumetric method was carried out by injecting known volumes of VOC liquids into a chamber equipped with two fans to mix the vapors and with an internal

temperature/relative humidity (RH) sensor. The sensor response was defined as the ratio R_a/R_g, where R_g and R_a are the measured response resistances in the test gas sample and in air, respectively.

3 Results and discussion

3.1 Characterization of the direct grown ZnO nanomaterials

The morphologies of the as-prepared products were firstly investigated by SEM. After the seeds preparation step, a dense film of ZnO seeds was located on the surface of the Al_2O_3 tube (Fig. 1). The seeds are sized in nm scale and very suitable for further growth of ZnO nanomaterials. Figure 2a–d is the SEM images of the ZnO nanomaterials prepared with NH_4F for 4 h. Therefore nanoprisms in several μm length with rhombus planes were generated upon the seeds film after it was incubated in the NH_4F growth solution for 4 h. And underneath the nanoprisms, random distributed nanosheets directly grown upon the seeds film could also be seen in an enlarged SEM image. From the cross-section view we can see that the nanoprisms are well contact with the seeds film, and the thickness is about 5 μm. And after calcinated in air at 300 °C for 3 h, no significant morphology changes have been found. Figure 2e–g shows the SEM images of the ZnO nanomaterials prepared with NH_4F for 8 h. Obviously, dense nanoprisms with rhobus planes outside are aligned along the surface of the Al_2O_3 tube. The size of the rhombus planes has covered a large range from hundred nm to several μm which could be further improved by changing the growth conditions such as pH value, concentration, temperature, etc. The cross-section SEM image also evidences the good adhesion between the ZnO nanoprisms and the seeds film which could generate favorable ohm and mechanical contact and be beneficial to gas sensing.

Figure 3 is the SEM images of the direct grown ZnO nanomaterials prepared with HMT. As shown in Fig. 3a–d, after 4h's growth, the surface of the sensor substrates is covered with nanosheets and nanorods. However, the distribution of the nanosheets and nanorods is rare and almost isolated which may cause a large resistance and a poor conductivity. And also no significant morphology changes have been found after calcination. Meanwhile, as the grown duration prolonged, flower-like nanorods assembled hierarchical structures were emerged upon the surface of the random distributed nanosheets and nanorods, and the corresponding SEM images are shown in Fig. 3e–h. The nanorods presents rough surface where small spikes are grown around the side planes. After calcination, the spikes are disappeared and the rough surface of the nanorods became more fine and smooth. And each nanorod has a well-defined hexagonal plane with a homogeneous diameter of approximately 200 nm. The morphology of the nanoflower hierarchical structures is in accordance with that of the precipitates collected from the growth solution (Fig. 4). The hierarchical nanostructures fabricated here makes the ZnO nanomaterials own large surface area and more deficiencies which are desirable characteristics for gas sensor.

Figure 5 shows the SEMs of the ZnO nanomaterials grown in Urea. As shown in Fig. 5a–d, the nanoflakes are uniform and homogenous with large size and density. Most of the nanoflakes stand uniformly on the surface and connect with each other to form a network. Figure 5e and f is the SEM images of ZnO nanomaterials grown in Urea with the reaction time of 8 h. It can be found obviously that nanourchins with $\sim$4 μm in diameter are covered the surface of the Al_2O_3 tubes. The ZnO nanourchins are assembled with nanoleaves which could be found in the precipitate collected in the solution (Fig. 6). After calcination, the morphology of the nanourchins is preserved but parts of them are collapsed into nanoleaves scattered on the surface. The cross-section view SEM images of the ZnO

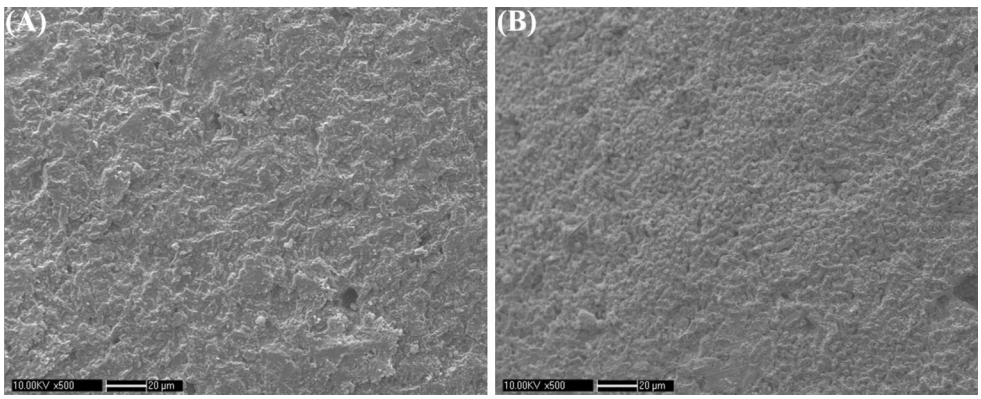

Fig. 1 The SEM images of **a** Al_2O_3 tube and **b** seeds film

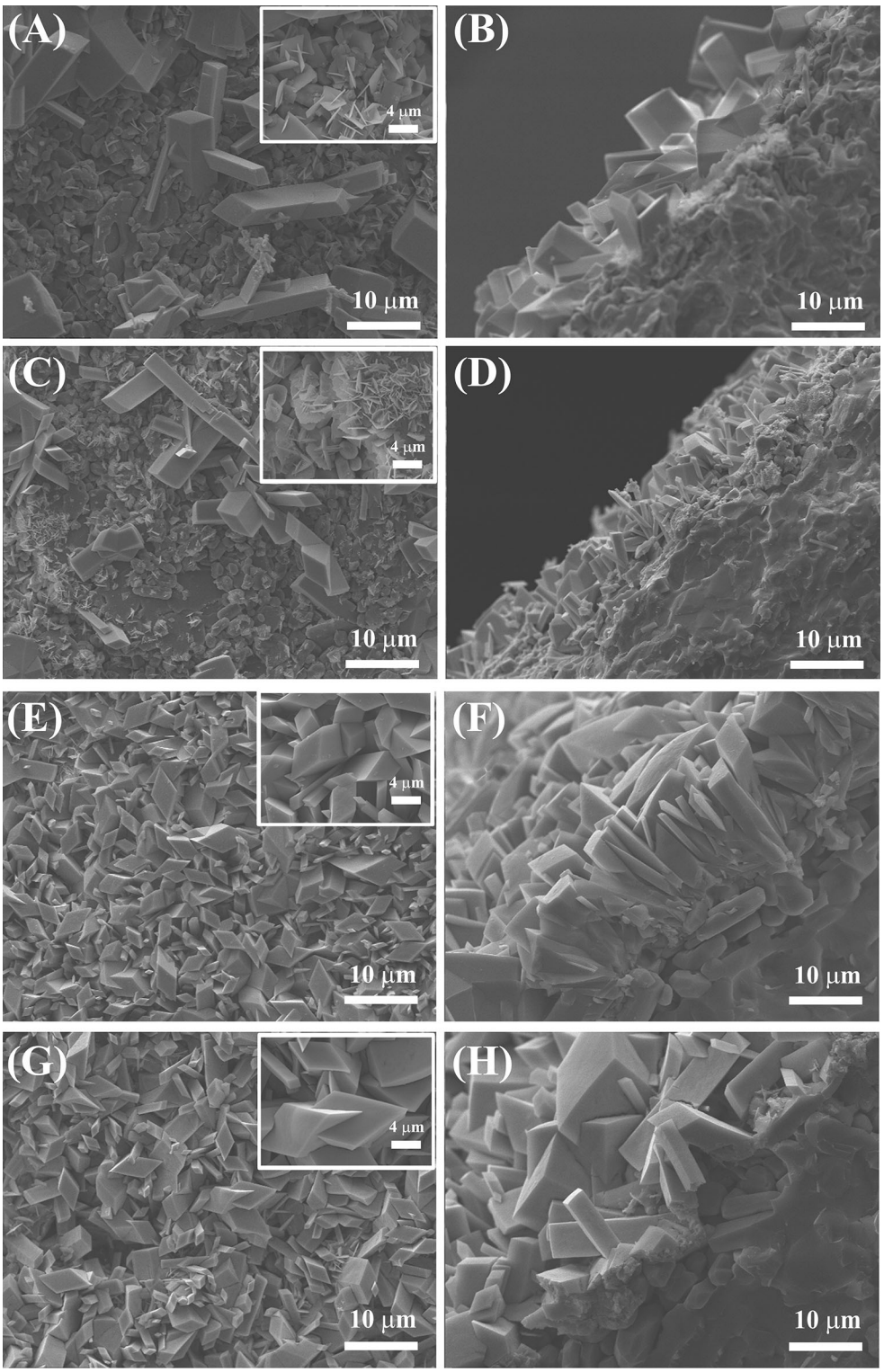

Fig. 2 The top and cross-section SEM images of the direct grown ZnO nanomaterials in NH_4F for **a**, **b** 4 h before calcination, **c**, **d** 4 h after calcination, **e**, **f** 8 h before calcination, and **g**, **h** 8 h after calcination. *Insets* are the corresponding SEM images in a higher magnitude

nanourchins prepared for 8 h is similar to that prepared for 4 h, so the corresponding images do not show here. Unfortunately, the nanourchins could not be found in the cross-section SEM images. One of the possible reasons is that the nanourchins are unstable contact with the seeds film or the upon-grown nanoflakes and could be easily

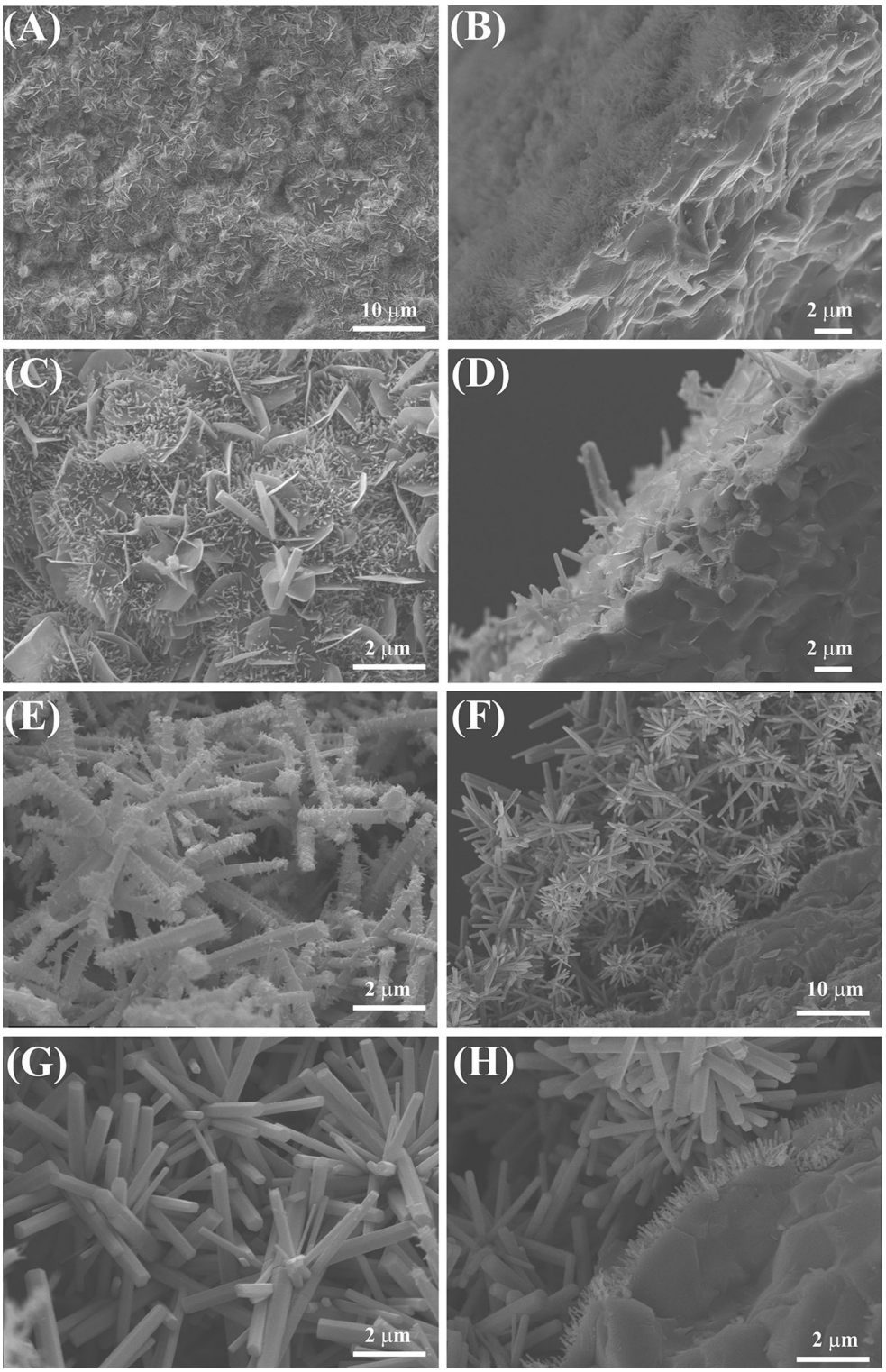

Fig. 3 The top and cross-section SEM images of the direct grown ZnO nanomaterials in HMT for **a**, **b** 4 h before calcination, **c**, **d** 4 h after calcination, **e**, **f** 8 h before calcination, and **g**, **h** 8 h after calcination

removed due to the violent operation during the SEM sample preparation step.

The crystal structures of the as-prepared products were characterized by XRD patterns as shown in Fig. 7. All of the diffraction peaks can be indexed to wurtzite ZnO (JCPDS No. 36-1451) which is the most stable and most common form [39]. From the results of SEM and XRD, it can be seen that the direct grown ZnO nanomaterials on the

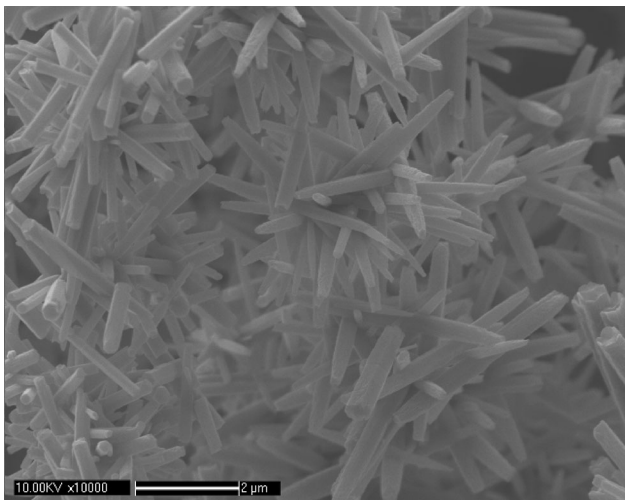

Fig. 4 The SEM image of the precipitates collected from the HMT growth solution

Al_2O_3 tube surface is realized successfully by a facile solution-processing technique, resulting in an improvement of surface area and ohm contact, which will greatly influence the gas sensing properties.

3.2 Gas sensing properties of the ZnO sensors

For the investigation of the gas sensing properties of the ZnO nanomaterials, the optimum working temperature should be determined at the very first. For this, the sensitivity of the ZnO nanomaterials sensors to 100 ppm ethanol were measured as a function of the working temperature and the results are shown in Fig. 8. The sensitivities to ethanol vapors continuously increase with increasing the working temperature until they reach their maximum at 320 °C. And a further increase of the temperature causes decrease of the sensitivities. The maximum sensitivities to 100 ppm ethanol vapors are 82, 143, 51, 200, 6 and 78 for the ZnO sensors prepared in NH_4F 4 h, NH_4F 8 h, HMT 4 h, HMT 8 h, Urea 4 h and Urea 8 h, respectively. Therefore, the optimal working temperature of 320 °C was chosen to further examine the characteristics of the ZnO nanomaterials sensors.

Figure 9 indicates a typical response profiles to investigate repeatability of the gas sensors after aged 10 days. It can be noted that all the sensors are in good reproducible run after seven cycles, which demonstrated a better repeatability of the sensors. The gas sensing properties of ZnO nanomaterials are in general based on n-type surface-dominant mechanism, in which adsorption and desorption processes occur at the surface of sensing materials [27]. When the ZnO nanomaterials is exposed to air, O_2 molecules are absorbed onto the surface of the ZnO nanomaterials and transformed to O_2^-, O^-, or O^{2-} depending on the working temperature. The absorption of O_2 traps free electrons from the conduction band of ZnO nanomaterials and causes the increase of resistance of the sensor. When the ZnO nanomaterials is exposed to a reducing gas like VOCs vapors, the VOCs molecules react with the absorbed oxygen anions and release the trapped electrons to the conduction band, leading to a decrease in the resistance. Thus, the active surface area and surface status of the sensing material play a crucial role in the gas sensing performance. ZnO nanomaterials with large surface area and abundant surface defects is expected to show excellent sensing performance.

In order to explore the VOCs detection properties of the ZnO sensors, the response to 100 ppm VOCs are recorded, and the results are shown in Fig. 10. Methanol, ethanol, acetone and acetonitrile are selected as the study subjects because of their wide and abused application in chemical laboratory. Obviously, all of the ZnO sensors present clear responses to the examined VOCs, especially methanol, ethanol and acetone. The ZnO sensor shows relative higher sensing responses to methanol, ethanol and acetone, lower responses to the acetonitrile. It seems that the ZnO sensors have selective sensing ability to the hydroxyl and carbonyl VOCs. Among the ZnO sensors, the ZnO prepared in the HMT system shows a better sensing response. Meanwhile, the ZnO grown time also reveals to be an important factor that influences the sensor responses. The ZnO sensor grown in HMT for 8 h shows the highest sensitivity to almost all of the VOCs, especially for ethanol which is about 4 fold higher than that for 4 h. Such enhancement could be attributed to the high surface area and deficiency of the hierarchical structures of the ZnO nanoflowers prepared in the HMT system. The similar sensitivity enhancement phenomenon could also be seen in the other two ZnO grown systems, however, their enhancement amplitude are lower than that in the HMT system.

Based on the excellent sensing performance of the ZnO nanomaterials, those VOCs have been exploited to investigate its potential applications. Figure 11 shows the dynamic response curves of the ZnO nanomaterials sensors to methanol, ethanol and acetone, respectively. It is obviously observed that the responses increase with the increase of VOCs vapor concentration, which can be obviously seen from their sensitivity *vs* concentration relationships in the Fig. 11b, d, f. The dynamic response curves also suggest that the ZnO nanomaterials prepared in the HMT system has better sensing properties. And all of the sensors were much sensitive to ethanol than others, which might be owed to the easier oxidation of hydroxyl group at that condition.

The response and recovery time are also important parameters for gas sensors. The response time is defined

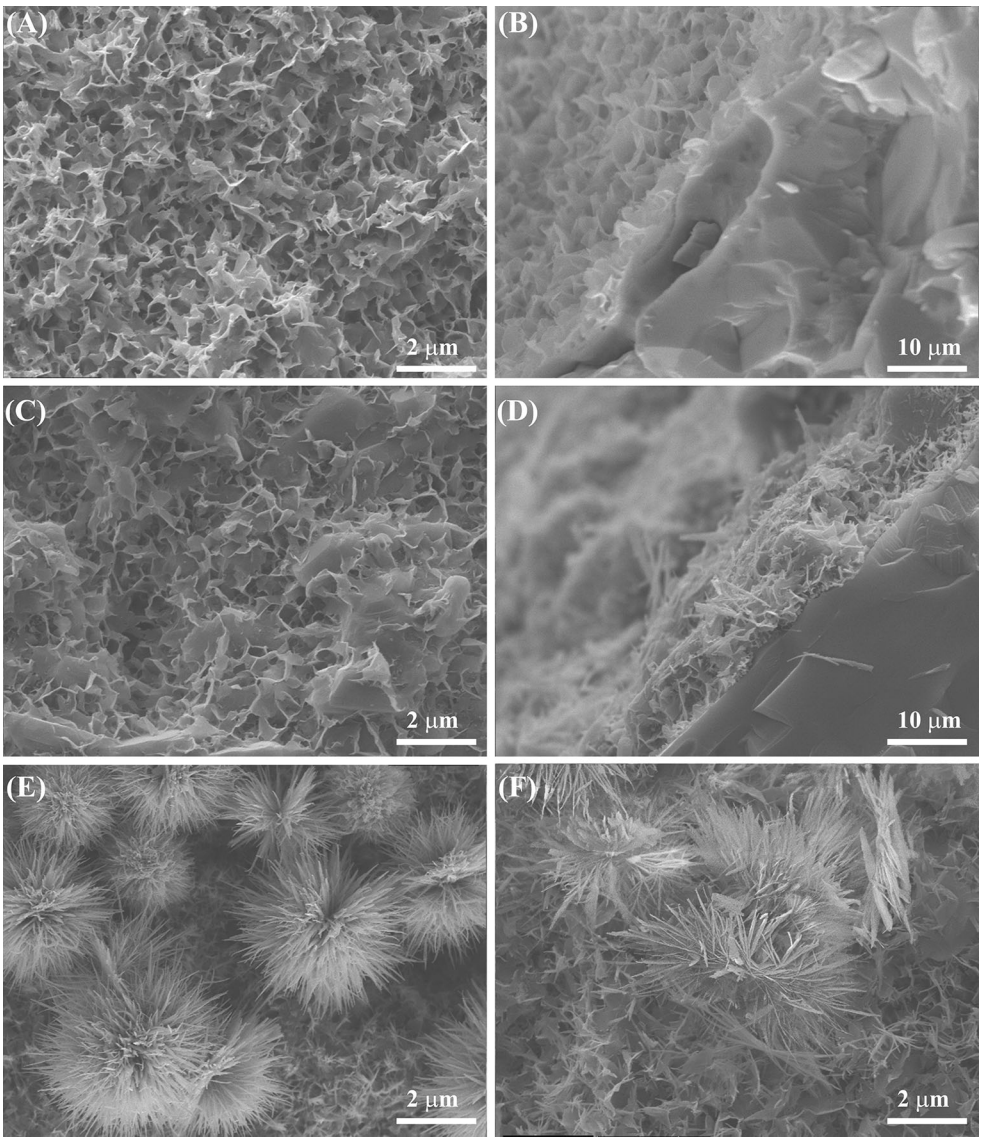

Fig. 5 The top and cross-section SEM images of the direct grown ZnO nanomateirals in urea for **a**, **b** 4 h before calcination, **c**, **d** 4 h after calcination, **e**, **f** 8 h before and after calcination

as the time required for the response signal to reach 90 % of the sample resistance after the introduction of the test gas. The recovery time is defined as the time needed to return to 10 % above the initial resistance in air after the test gas has been released. The transient response of the ZnO nanomaterials sensors toward 100 ppm ethanol are shown in Fig. 12. When the sensors were exposed to ethanol vapor, the response increased rapidly, which the response signal recovered quickly to the baseline when the sensor was disengaged form the tested circumstance. It is suggesting that the ZnO nanomateirals are effective to capture VOCs molecules and to desorb them rapidly through the nanostructures. To 100 ppm ethanol, the ZnO nanomaterial prepared in the NH_4F system displays the shortest response time ($\sim$5 s), however, those prepared from urea shows the shortest recovery time ($\sim$15 s), and the ZnO nanomaterial prepared from HMT shows slightly longer response and recovery time. Beside the enhancement of the sensitivity, the response and recovery time seems to show a prolong trends when the grown duration was prolonged. In order to demonstrate the superior gas sensing properties of the direct grown ZnO nanomaterials, a comparison of the sensor performances is summarized in Table 1. Obviously, the hierarchical nanostructures prepared in this work exhibit the highest sensitivity to ethanol, and also

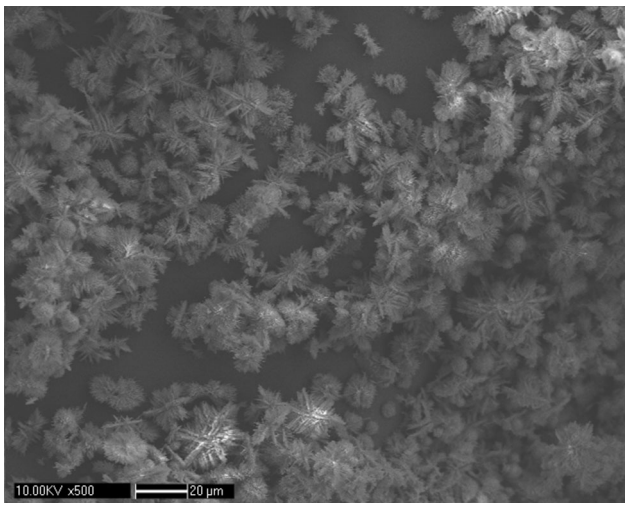

Fig. 6 The SEM image of the precipitates collected from the urea growth solution

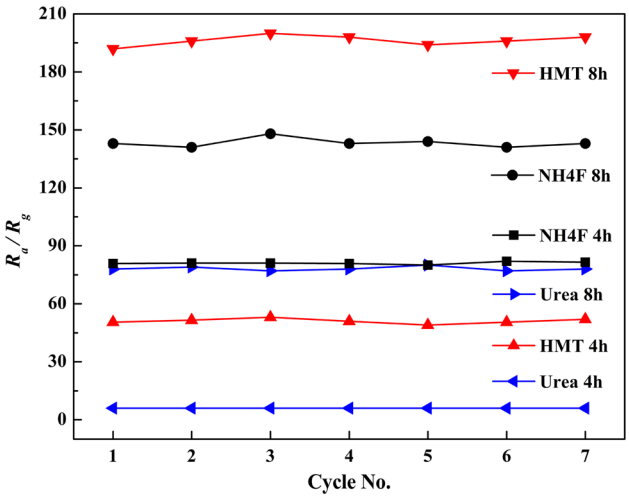

Fig. 9 The repeatability testing of the ZnO sensors towards 100 ppm ethanol at 320 °C

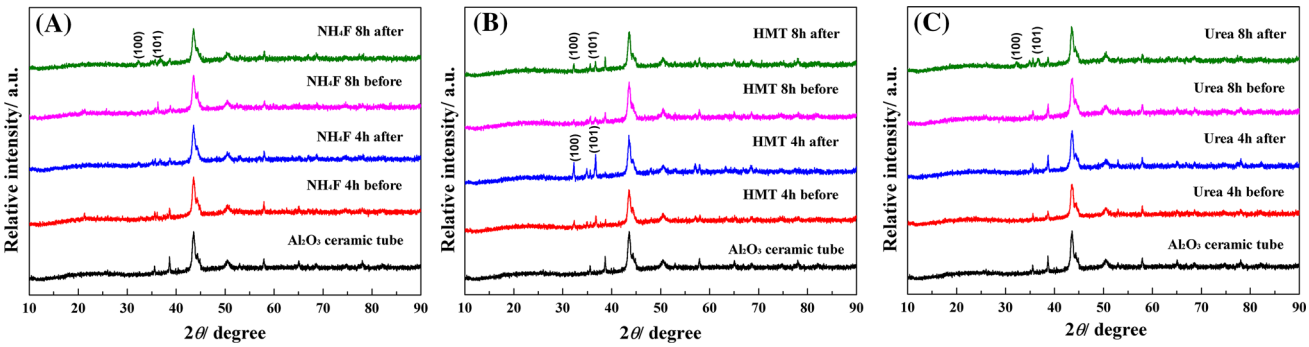

Fig. 7 The XRD *curves* of the direct grown ZnO nanomaterials in **a** NH_4F, **b** HMT and **c** urea. The peaks are indexed to ZnO (JCPDS No. 36-1451)

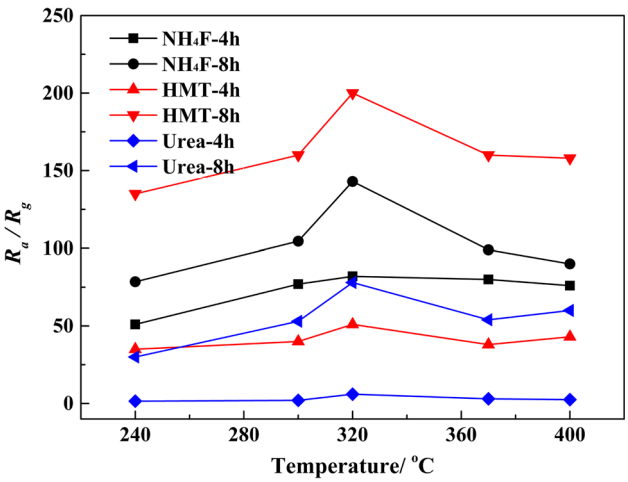

Fig. 8 The influence of working temperature on the ZnO sensors response of 100 ppm ethanol

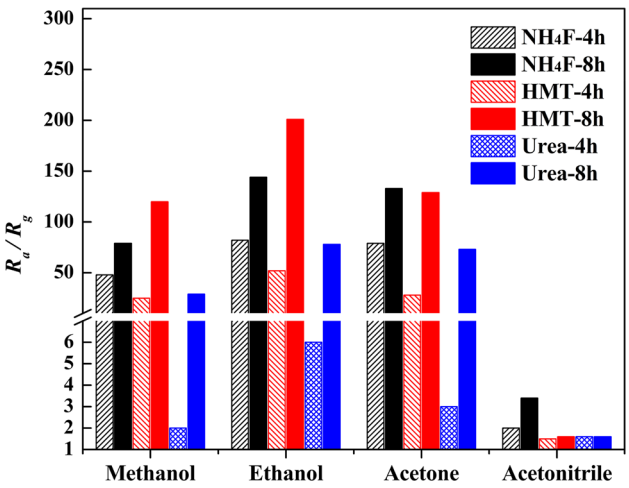

Fig. 10 The response of ZnO sensors to 100 ppm VOCs at 320 °C

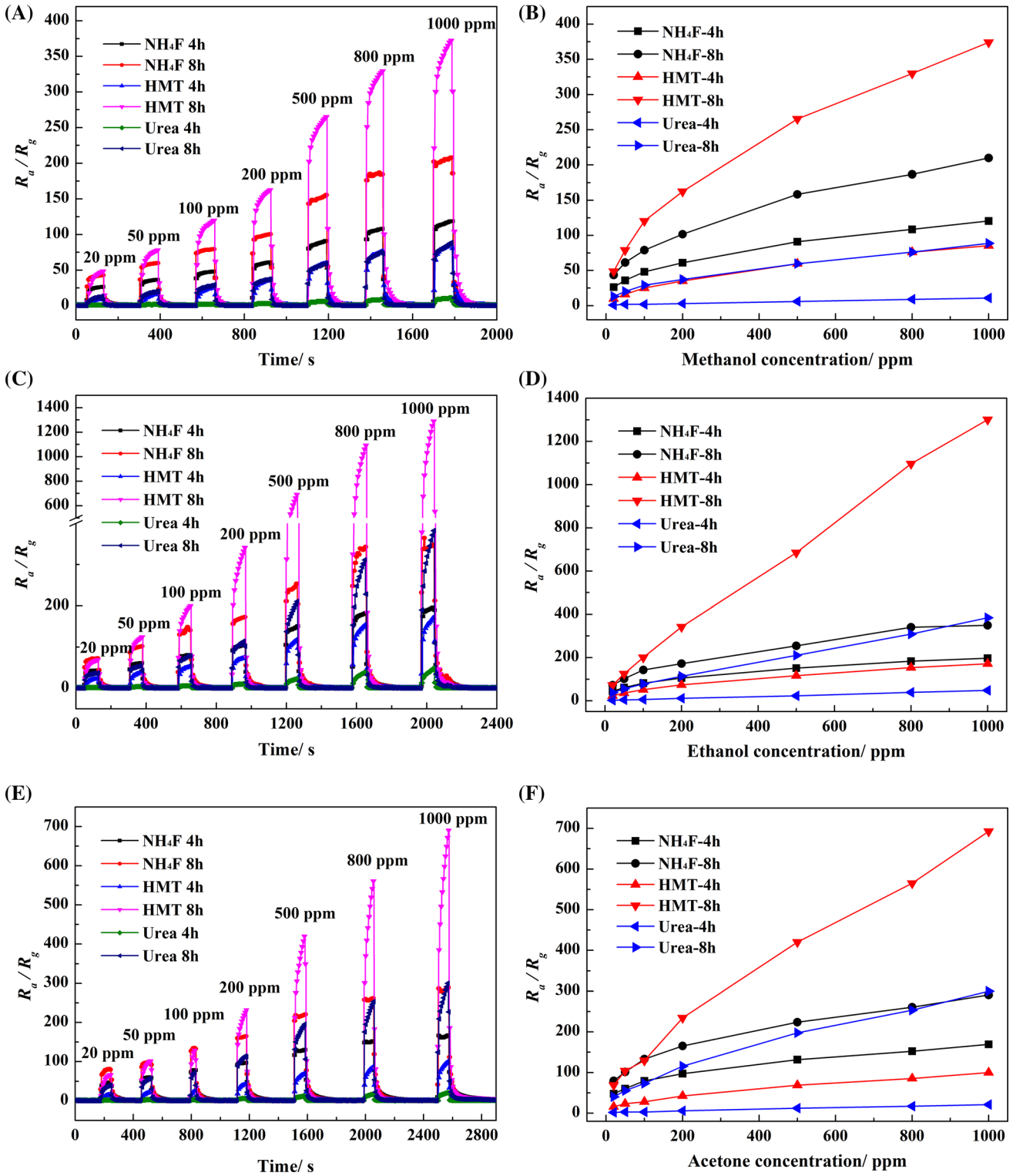

Fig. 11 Dynamic response curves and the corresponding relationship of **a**, **b** methanol, **c**, **d** ethanol, and **e**, **f** acetone on ZnO sensors at 320 °C

moderate response and recovery performances. However, compared to the others, the working temperature, response and recovery time are still need to be further improved by optimizing the synthesize conditions or successful doping. And the relating experiment is carrying out in our laboratory.

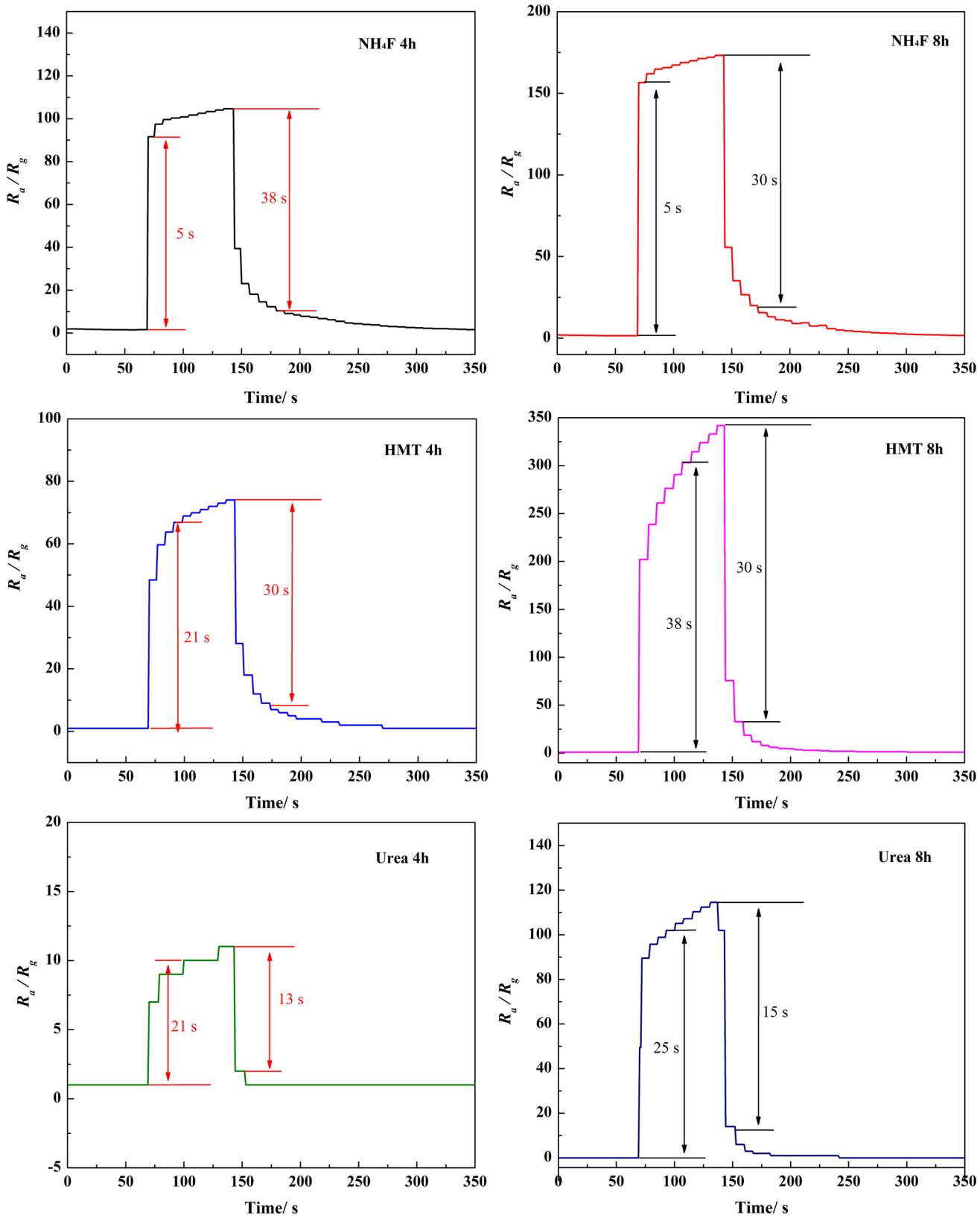

Fig. 12 The response and recovery times of ZnO nanomaterials sensors on exposure to 100 ppm of ethanol vapor

Table 1 Gas responses to ethanol of the ZnO nanomaterials sensors in the present study and those reported in the literature

Sensing materials	Ammonia source	Method	[CH_3CH_2OH] (ppm)	R_a/R_g	T_{sens} (°C)	$t_{response}/t_{recovery}$	References
Nanosheets assembled nanoflowers	Urea	One-pot hydrothermal method	100	8.5	220	10 s/80 s	[40]
Porous nanosheets network	Ethylenediamine	Two step seeds-assistant hydrothermal method	100	18	320	-/-	[26]
Porous nanosheets network	HMT	One step hydrothermal method	100	40	400	8 s/17 s	[27]
Nanorods array	HMT	Two step seeds-assistant solution method	100	67	370	10 s/10 s	[34]
Nanopillar	HMT	Two step seeds-assistant hydrothermal method	100	18.3	350	–/–	[35]
Mesoporous rhombus-shaped nanorods	HMT-NH_4F	Two step seeds-assistant hydrothermal method	100	11.8	300	4 s/7 s	[36]
Rhombus-shaped nanoprisms	NH4F-8 h	Two step seeds-assistant solution method	100	144	320	5 s/30 s	This work
Nanorods assembled nanoflowers	HMT-8 h			200		38 s/30 s	
Nanoleaves constructed nanourchins	Urea-8 h			78		25 s/15 s	

4 Conclusions

In summary, direct grown ZnO nanomaterials on ceramic tubes have been prepared by two step seeds-assisted solution method using NH_4F, HMT and urea as the ammonia source. The ZnO nanomaterials present different morphologies and hierarchical structures where rhombus-shaped nanoprisms, nanorods assembled nanoflowers and nanoleaves constructed nanourchins are obtained in NH_4F, HMT and urea, respectively. All of the ZnO nanomaterials show the optimal working temperature at 320 °C and excellent repeatability. Gas sensing experiments reveal that the ZnO nanomateirals perform high responses and fast response-recovery to VOCs, especially for the nanorods assembled nanoflowers prepared in the HMT. Furthermore, the ZnO nanoprisms prepared in the NH_4F system displays the shortest response time ($\sim$5 s) and the ZnO nanourchins prepared from Urea shows the shortest recovery time ($\sim$15 s), however, the ZnO nanoflowers prepared from HMT shows slightly longer response and recovery time. It is believed that the superior gas sensing properties of the direct grown ZnO nanomaterials could be further utilized in indoor air quality detection.

Acknowledgments This study was financially supported by the Foundation of CAEP (426030302).

References

1. A. Menzel, K. Subannajui, F. Güder, D. Moser, O. Paul, M. Zacharias, Multifunctional ZnO-nanowire-based sensor. Adv. Funct. Mater. **21**, 4342–4348 (2011)
2. M. Chen, Z. Wang, D. Han, F. Gu, G. Guo, High-sensitivity NO_2 gas sensors based on flower-like and tube-like ZnO nanomaterials. Sens. Actuators B Chem. **157**, 565–574 (2011)
3. E. Şennik, S. Kerli, Ü. Alver, Z.Z. Öztürk, Effect of fluorine doping on the NO_2-sensing properties of ZnO thin films. Sens. Actuators B Chem. **216**, 49–56 (2015)
4. R.K. Sonker, S.R. Sabhajeet, S. Singh, B.C. Yadav, Synthesis of ZnO nanopetals and its application as NO_2 gas sensor. Mater. Lett. **152**, 189–191 (2015)
5. M. Chen, Z. Wang, D. Han, F. Gu, G. Guo, Porous ZnO polygonal nanoflakes: synthesis, use in high-sensitivity NO_2 gas sensor, and proposed mechanism of gas sensing. J. Phys. Chem. C **115**, 12763–12773 (2011)
6. H. Gong, J.Q. Hu, J.H. Wang, C.H. Ong, F.R. Zhu, Nano-crystalline Cu-doped ZnO thin film gas sensor for CO. Sens. Actuators B Chem. **115**, 247–251 (2006)
7. M. Hjiri, L. El Mir, S.G. Leonardi, A. Pistone, L. Mavilia, G. Neri, Al-doped ZnO for highly sensitive CO gas sensors. Sens. Actuators B Chem. **196**, 413–420 (2014)
8. N.D. Khoang, H.S. Hong, D.D. Trung, N.V. Duy, N.D. Hoa, D.D. Thinh, N.V. Hieu, On-chip growth of wafer-scale planar-type ZnO nanorod sensors for effective detection of CO gas. Sens. Actuators B Chem. **181**, 529–536 (2013)
9. V.A. Minh, L.A. Tuan, T.Q. Huy, V.N. Hung, N.V. Quy, Enhanced NH_3 gas sensing properties of a QCM sensor by increasing the length of vertically orientated ZnO nanorods. Appl. Surf. Sci. **265**, 458–464 (2013)
10. P. Sundara Venkatesh, P. Dharmaraj, V. Purushothaman, V. Ramakrishnan, K. Jeganathan, Point defects assisted NH_3 gas sensing properties in ZnO nanostructures. Sens. Actuators B Chem. **212**, 10–17 (2015)
11. K. Diao, M. Zhou, J. Zhang, Y. Tang, S. Wang, X. Cui, High response to H_2S gas with facile synthesized hierarchical ZnO microstructures. Sens. Actuators B Chem. **219**, 30–37 (2015)
12. Z.S. Hosseini, A. Mortezaali, A. Iraji zad, S. Fardindoost, Sensitive and selective room temperature H_2S gas sensor based on Au sensitized vertical ZnO nanorods with flower-like structures. J. Alloys Comp. **628**, 222–229 (2015)
13. Z.S. Hosseini, A.I. Zad, A. Mortezaali, Room temperature H_2S gas sensor based on rather aligned ZnO nanorods with flower-like structures. Sens. Actuators B Chem. **207A**, 865–871 (2015)

14. A. Mortezaali, R. Moradi, The correlation between the substrate temperature and morphological ZnO nanostructures for H_2S gas sensors. Sens. Actuators A Phys. **206**, 30–34 (2014)
15. N.H. Al-Hardan, M.J. Abdullah, A. Abdul Aziz, H. Ahmad, L.Y. Low, ZnO thin films for VOC sensing applications. Vacuum **85**, 101–106 (2010)
16. I. Elmi, S. Zampolli, E. Cozzani, F. Mancarella, G.C. Cardinali, Development of ultra-low-power consumption MOX sensors with ppb-level VOC detection capabilities for emerging applications. Sens. Actuators B Chem. **135**, 342–351 (2008)
17. N. Kilinc, O. Cakmak, A. Kosemen, E. Ermek, S. Ozturk, Y. Yerli, Z.Z. Ozturk, H. Urey, Fabrication of 1D ZnO nanostructures on MEMS cantilever for VOC sensor application. Sens. Actuators B Chem. **202**, 357–364 (2014)
18. Y.V. Kaneti, J. Yue, X. Jiang, A. Yu, Controllable synthesis of ZnO nanoflakes with exposed (1010) for enhanced gas sensing performance. J. Phys. Chem. C **117**, 13153–13162 (2013)
19. W. Guo, T. Liu, H. Zhang, R. Sun, Y. Chen, W. Zeng, Z. Wang, Gas-sensing performance enhancement in ZnO nanostructures by hierarchical morphology. Sens. Actuators B Chem. **166–167**, 492–499 (2012)
20. K.M. Kim, H.R. Kim, K.I. Choi, H.J. Kim, J.H. Lee, ZnO hierarchical nanostructures grown at room temperature and their C_2H_5OH sensor applications. Sens. Actuators B Chem. **155**, 745–751 (2011)
21. S. Ma, R. Li, C. Lv, W. Xu, X. Gou, Facile synthesis of ZnO nanorod arrays and hierarchical nanostructures for photocatalysis and gas sensor applications. J. Hazard. Mater. **192**, 730–740 (2011)
22. M.R. Alenezi, T.H. Alzanki, A.M. Almeshal, A.S. Alshammari, M.J. Beliatis, S.J. Henley, S.R.P. Silva, Hierarchically designed ZnO nanostructure based high performance gas sensors. RSC Adv **4**, 49521–49528 (2014)
23. M.R. Alenezi, S.J. Henley, N.G. Emerson, S.R.P. Silva, From 1D and 2D ZnO nanostructures to 3D hierarchical structures with enhanced gas sensing properties. Nanoscale **6**, 235–247 (2014)
24. H. Zhang, R. Wu, Z. Chen, G. Liu, Z. Zhang, Z. Jiao, Self-assembly fabrication of 3D flower-like ZnO hierarchical nanostructures and their gas sensing properties. CrystEngComm **14**, 1775–1782 (2012)
25. Z. Chen, Z. Lin, Y. Hong, N. Li, M. Xu, Hydrothermal synthesis of hierarchically porous Rh-doped ZnO and its high gas sensing performance to acetone. J. Mater. Sci. Mater. Electron. (2015). doi:10.1007/s10854-015-4069-x
26. D. Ju, H. Xu, Z. Qiu, J. Guo, J. Zhang, B. Cao, Highly sensitive and selective triethylamine-sensing properties of nanosheets directly grown on ceramic tube by forming NiO/ZnO PN heterojunction. Sens. Actuators B Chem. **200**, 288–296 (2014)
27. D.X. Ju, H.Y. Xu, J. Zhang, J. Guo, B.Q. Cao, Direct hydrothermal growth of ZnO nanosheets on electrode for ethanol sensing. Sens. Actuators B Chem. **201**, 444–451 (2014)
28. S.L. Zhang, J.O. Lim, J.S. Huh, J.S. Noh, W. Lee, Two-step fabrication of ZnO nanosheets for high-performance VOCs gas sensor. Curr. Appl. Phys. **13S2**, S156–S161 (2013)
29. W. Guo, T. Liu, Z. Guo, W. Zeng, Y. Chen, Z. Wang, Hydrothermal synthesis of ultrathin ZnO nanosheets and their gas-sensing properties. J. Mater. Sci. Mater. Electron. **24**, 1764–1769 (2013)
30. J. Du, R. Zhao, S. Chen, H. Wang, J. Li, Z. Zhu, Self-assembly of gridlike zinc oxide lamellae for chemical-sensing applications. ACS Appl Mater. Interfaces **7**, 5870–5878 (2015)
31. A. Zou, L. Hu, Y. Qiu, G. Cao, J. Yu, L. Wang, H. Zhang, B. Yin, L. Xu, High performance of 1-D ZnO microwire with curve-side hexagon as ethanol gas sensor. J. Mater. Sci. Mater. Electron. **26**, 4908–4912 (2015)
32. F. Li, H. Zhang, L. Hu, Y. Luo, Y. Zhao, Y. Qiu, J. Ji, L. Yue, A novel ethanol gas sensor based on ZnO microwire. J. Mater. Sci. Mater. Electron. **24**, 4812–4816 (2013)
33. D. Calestani, R. Mosca, M. Zanichelli, M. Villani, A. Zappettini, Aldehyde detection by ZnO tetrapod-based gas sensors. J. Mater. Chem. **21**, 15532–15536 (2011)
34. S. Tian, F. Yang, D. Zeng, C. Xie, Solution-processed gas sensors based on ZnO nanorods array with an exposed (0001) facet for enhanced gas-sensing properties. J. Phys. Chem. C **116**, 10586–10591 (2012)
35. L.J. Bie, X.N. Yan, J. Yin, Y.Q. Duan, Z.H. Yuan, Nanopillar ZnO gas sensor for hydrogen and ethanol. Sens. Actuators B Chem. **126**, 604–608 (2007)
36. Z. Wen, L. Zhu, Z. Zhang, Z. Ye, Fabrication of gas sensor based on mesoporous rhombus-shaped ZnO rod arrays. Sens. Actuators B Chem. **208**, 112–121 (2015)
37. W. Guo, T. Liu, L. Huang, H. Zhang, Q. Zhou, W. Zeng, HMT assisted hydrothermal synthesis of various ZnO nanostructures: structure, growth and gas sensor properties. Physica E **44**, 680–685 (2011)
38. X. Tian, L. Yang, X. Qing, K. Yu, X. Wang, Trace level detection of hydrogen gas using birnessite-type manganese oxide. Sens. Actuators B Chem. **207A**, 34–42 (2015)
39. F. Grasset, N. Saito, D. Li, D. Park, I. Sakaguchi, N. Ohashi, H. Haneda, T. Roisnel, S. Mornet, E. Duguet, Surface modification of zinc oxide nanoparticles by aminopropyltriethoxysilane. J. Alloys Comp. **360**, 298–311 (2003)
40. F. Meng, N. Hou, S. Ge, B. Sun, Z. Jin, W. Shen, L. Kong, Z. Guo, Y. Sun, H. Wu, C. Wang, M. Li, Flower-like hierarchical structures consisting of porous single-crystalline ZnO nanosheets and their gas sensing properties to volatile organic compounds (VOCs). J. Alloys Comp. **626**, 124–130 (2015)